Perturbative Theory of Off-Specular Synchrotron Mössbauer Reflectometry

L. Deák,[1,*] L. Bottyán,[1] D.L. Nagy,[1] H. Spiering,[2] Yu.N. Khaidukov,[3] and Y. Yoda[4]

[1]*KFKI Research Institute for Particle and Nuclear Physics, P.O.B. 49, H-1525 Budapest, Hungary*

[2]*Institut für Anorganische und Analytische Chemie, Johannes Gutenberg Universität Mainz, Staudinger Weg 9, D-55099 Mainz, Germany*

[3]*Joint Institute for Nuclear Research, 141980, Dubna, Moscow Region, Russia*

[4]*SPring-8 JASRI, 1-1-1 Kouto Mikazuki-cho Sayo-gun Hyogo 679-5198, Japan*

(Dated: October 24, 2006)

Abstract

Synchrotron Mössbauer Reflectometry (SMR), the grazing-incidence nuclear resonant scattering of synchrotron radiation, can be applied to perform depth-selective phase analysis and to determine the isotopic and magnetic structure of thin films and multilayers. Off-specular SMR provides information on the lateral structure of multilayers. A theoretical description of off-specular SMR based on the Distorted-Wave Born Approximation is presented. Off-specular SMR and polarized neutron reflectivity curves of an antiferromagnetic $\left[^{57}\mathrm{Fe}/\%\mathrm{Cr}\right]$ multilayer are calculated and compared. Experimental '$2\theta - \omega$' SMR scans are compared with the theory.

PACS numbers: PACS: 42.25-p, 61.10.Kw, 61.12.Ha, 75.25.+z

Keywords:

I. INTRODUCTION

Grazing-incidence reflection of x-rays[1,2] and neutrons[1,2,3,4,5] from flat surfaces (x-ray and neutron reflectometry, as well as grazing-incidence soft x-ray resonant magnetic scattering[6,7]) have been widely used to investigate the chemical, isotopic and magnetic structure of thin films and multilayers (ML).[8,9,10] The sensitivity of nuclear resonant scattering (NRS) of synchrotron radiation to hyperfine interactions renders possible a special kind of x-ray reflectometry, a method that we shall call henceforth Synchrotron Mössbauer Reflectometry (SMR).[11,14] SMR combines the sensitivity of Mössbauer spectroscopy to hyperfine interactions with the depth information yielded by reflectometry. Like other NRS experiments, SMR contains the hyperfine interaction information in the quantum beats of the time response that follows the excitation of the system by the synchrotron radiation pulse. Time-differential (TD) SMR is a grazing-incidence time-domain NRS experiment performed at one or at a series of different grazing angles. In a time-integral (TI) SMR experiment all delayed (i.e., nuclear resonantly scattered) photons are counted as a function of the grazing angle. This method is very similar to polarized neutron reflectometry (PNR) and yields integral hyperfine depth profile and superstructure information. Specular SMR has by now become an established technique.[12,13,14,15]

The specularly reflected radiation from a stratified system is insensitive to the lateral structure; it depends solely on the lateral averages of the material parameters[1] for the coherence volume. In particular, using monochromatic radiation of infinite coherence length, the magnetic contrast (AF Bragg peak) of an antiferromagnetic (AF) multilayer with compensated domains would be missing from the specular reflectivity. However, this is not the case, since the coherent averaging has to be performed for the finite coherence volume of the radiation determined by the experimental setup and such contributions are to be added incoherently.[18] For studying lateral inhomogeneities, such as structural roughness, magnetic domains, etc., diffuse scattering, i.e. off-specular reflectometry is used. Off-specular non-polarized[10] and polarized neutron reflectometry,[3,9] soft-x-ray resonant magnetic diffuse scattering[8] and, recently, off-specular SMR have been used to estimate the domain-size distribution and to follow domain transformations in AF-coupled magnetic MLs.[16]

The theory of the off-specular *neutron* reflectometry based on the Distorted-Wave Born Approximation[17] (DWBA) has been published earlier.[18,19,20,21] DWBA perturbatively de-

termines the diffuse (off-specular) field[22] around the specular field, the latter being easily calculated, even for general stratified media, by suitable matrix methods.[18,19,23,24,25,26] The optical solution of the specular SMR problem is also well-known.[15,26,27,28,29,30,31,32,33,34] The idea to apply the DWBA technique to describe off-specular SMR experiments is therefore plausible. However, as we shall see, due to strong energy dependence of the coherent field and the susceptibilities and the consequent temporal character of SMR, this approach is not a trivial application of the existing theory. In the present paper, based on perturbation theory, we work out a theory description for off-specular SMR.

Starting from Lax' general theory[1] and from the common optical formalism of polarized neutron and Mössbauer reflectometry,[26] an expression for diffuse scattering of electromagnetic and/or quantum mechanical particle waves on laterally inhomogeneous stratified media is obtained. From the point of view of specular reflection, the set of discrete atomic scattering centers can be described/replaced by a homogeneous index of refraction n and solving the scattering problem is equivalent to solving the wave equation.[1] This approach is valid only if the direction of the scattered wave is far from the direction of low-index atomic Bragg reflections. In this paper we shall study the grazing-incidence limit, for which the index of refraction approximation is valid.[15,29,32,33,34]

The model systems of the present paper are multilayers and thin films, i.e., stratified media, having lateral inhomogeneities on the mesoscopic scale, i.e., unlike in case of surface roughness, at distances much larger then the atomic distances. In each homogeneous part around position $\mathbf{r}$ an index of refraction $n(\mathbf{r})$ is defined. Since n for both slow neutrons and X-rays differs only slightly from the 2×2 unit matrix I, the susceptibility $\chi(\mathbf{r}) = 2[n(\mathbf{r}) - I]$ can be conveniently used.[26]

II. OFF-SPECULAR SCATTERING

Using the index-of-refraction approximation in each homogeneous part of the system the solution of the inhomogeneous wave equation

$$\left[\Delta + k^2 I\right] \Psi(\mathbf{r}) = -k^2 \chi(\mathbf{r}) \Psi(\mathbf{r}) \tag{2.1}$$

yields $\Psi(\mathbf{r})$, representing the two components of the photon field or the neutron quantum mechanical spinor state at position $\mathbf{r}$, with k being the wave number in vacuum. In a

stratified medium we compose the susceptibility function

$$\chi(\mathbf{r}) = \sum_{l=1}^{S} \chi_l\left(\mathbf{r}_\parallel\right), \tag{2.2}$$

as the sum of the susceptibility functions of the individual layers $l..l = 1..S$, the last layer S is the substrate) depending solely on th in-plane coordinate, $\mathbf{r}_\parallel$.

If the homogeneous parts of the system are large compared to the wavelength, we may assume that the exact solution $\Psi(\mathbf{r})$ is close to the solution $\Psi_{\text{coh}}(\mathbf{r})$ of the coherent (specular) field equation[1]

$$\left[\Delta + k^2 I\right] \Psi_{\text{coh}}(\mathbf{r}) = -k^2 \sum \overline{\chi}_l \Psi_{\text{coh}}(\mathbf{r}), \tag{2.3}$$

which is obtained from Eq.(2.1) by replacing the susceptibilities $\chi_l\left(\mathbf{r}_\parallel\right)$ by the average susceptibility $\overline{\chi}_l$ of each layer l. In order to arrive at a perturbative equation, the sum $-k^2 \sum \overline{\chi}_l \Psi(\mathbf{r})$ is added and subtracted on the right-hand side of Eq.(2.1)

$$\left[\Delta + k^2 I\right] \Psi(\mathbf{r}) = -k^2 \sum \overline{\chi}_l \Psi(\mathbf{r}) - k^2 \sum \left[\chi_l\left(\mathbf{r}_\parallel\right) - \overline{\chi}_l\right] \Psi(\mathbf{r}). \tag{2.4}$$

For homogeneous layers $\chi_l\left(\mathbf{r}_\parallel\right) = \overline{\chi}_l$ the second sum vanishes on the right, so that Eq.(2.4) reduces is to Eq.(2.3), the basic equation of specular reflectometry.[21,26,32,35] The general solutions of Eq.(2.4) are looked for in a form

$$\Psi(\mathbf{r}) = \Psi_{\text{coh}}(\mathbf{r}) + \Psi_{\text{off}}(\mathbf{r}), \tag{2.5}$$

where $\Psi_{\text{coh}}(\mathbf{r})$ is the coherent field, which vanishes in any non-specular direction, and $\Psi_{\text{off}}(\mathbf{r})$ is the off-specular field. Substituting Eq.(2.5) into Eq.(2.4) and taking Eq.(2.3) into account

$$\left[\Delta + k^2 I\right] \Psi_{\text{off}}(\mathbf{r}) = -k^2 \sum \left[\chi_l\left(\mathbf{r}_\parallel\right) - \overline{\chi}_l\right] \Psi_{\text{coh}}(\mathbf{r}) - k^2 \sum \chi_l\left(\mathbf{r}_\parallel\right) \Psi_{\text{off}}(\mathbf{r}). \tag{2.6}$$

The coherent field $\Psi_{\text{coh}}(\mathbf{r})$, the solution of Eq.(2.3), is obtained by the optical method[26] as

$$\Psi_{\text{coh}}(\mathbf{k}, \mathbf{r}) = T\left(\mathbf{k}_\perp, \mathbf{r}_\perp\right) \Psi^{\text{in}} \exp\left(i\mathbf{k}_\parallel \cdot \mathbf{r}_\parallel\right) \tag{2.7}$$

(see Appendix A), where $\perp$ and $\parallel$ denote the out-of-plane and in-plane components of the respective vectors and Ψ^{in} is the amplitude of the incident plane wave of wave number vector $\mathbf{k} = \left(\mathbf{k}_\perp, \mathbf{k}_\parallel\right)$. Now we introduce the "cumulative transmittance" of the upper layer of the reflecting film of thickness $\mathbf{r}_\perp$ by:

$$T\left(\mathbf{k}_\perp, \mathbf{r}_\perp\right) = L^{[21]}\left(\mathbf{k}_\perp, \mathbf{r}_\perp\right)\left[I - R_{\mathrm{sp}}\left(\mathbf{k}_\perp\right)\right] + L^{[22]}\left(\mathbf{k}_\perp, \mathbf{r}_\perp\right)\left[I + R_{\mathrm{sp}}\left(\mathbf{k}_\perp\right)\right]. \tag{2.8}$$

$R_{\mathrm{sp}}\left(\mathbf{k}_\perp\right)$ is the 2×2 specular reflectivity matrix of the system[26], $L^{[21]}\left(\mathbf{k}_\perp, \mathbf{r}_\perp\right)$ and $L^{[22]}\left(\mathbf{k}_\perp, \mathbf{r}_\perp\right)$ are the respective 2×2 submatrices of the 4×4 characteristic matrix[26,32] L at depth $\mathbf{r}_\perp$ for an incoming plain wave defined by $\mathbf{k}_\perp$.

The physical interpretation of Eq.(2.6) is seen from its right-hand side, where the first term gives the source of the off-specular radiation, and the second term shows that the off-specular field is scattered by the whole multilayer. The off-specular field arises from the coherent field at the lateral inhomogeneities, namely from the regions, where the susceptibility χ differs from its average value $\overline{\chi}$. Eq.(2.6) can be solved up to arbitrary accuracy applying higher-order Born approximations.

As a first approximation the second term of the right-hand side of Eq.(2.6) is neglected, so the solution can be obtained by using the Green-function technique,

$$\Psi_{\mathrm{off}}\left(\mathbf{k}, \mathbf{r}\right) = \frac{k^2}{4\pi} \sum_l \int \mathrm{d}^3\mathbf{r}' \, \frac{\exp\left(ikR\right)}{R} \left[\chi_l\left(\mathbf{r}'_\parallel\right) - \overline{\chi_l}\right] \Psi_{\mathrm{coh}}\left(\mathbf{k}, \mathbf{r}'\right), \tag{2.9}$$

where $R = \left|\mathbf{r} - \mathbf{r}'\right|$. The approximation requires $\left\|\Psi_{\mathrm{coh}}\left(\mathbf{r}\right)\right\| \gg \left\|\Psi_{\mathrm{off}}\left(\mathbf{r}\right)\right\|$, which condition is feasible in the vicinity of the specular direction for magnetic multilayers of large enough homogeneous domain size[16,20] so that the exact solution $\Psi\left(\mathbf{r}\right)$ is close to the coherent field $\Psi_{\mathrm{coh}}\left(\mathbf{r}\right)$.

Far from the scatterer the Fraunhofer approximation

$$\frac{\exp\left(ikR\right)}{R} \approx \frac{\exp\left(ikr\right)}{r} \exp\left(-i\mathbf{k}' \cdot \mathbf{r}'\right) \tag{2.10}$$

is applied ($\mathbf{k}'$ being the wave number vector of the outgoing plane wave). The final result reads

$$\Psi_{\mathrm{off}}\left(\mathbf{k}, \mathbf{r} = \frac{\mathbf{k}'}{k} r\right) = \sqrt{\frac{\pi}{2}} \frac{k^2}{r} \exp\left(ikr\right) \sum_l S_l\left(\mathbf{K}_\parallel\right) T_l\left(\mathbf{k}_\perp, \mathbf{k}'_\perp\right) \Psi^{\mathrm{in}}, \tag{2.11}$$

where

$$T_l\left(\mathbf{k}_\perp, \mathbf{k}'_\perp\right) = \frac{1}{\sqrt{2\pi}} \int\limits_{Z_l} \mathrm{d}\mathbf{r}_\perp \exp\left(-i\mathbf{k}'_\perp \mathbf{r}_\perp\right) T\left(\mathbf{k}_\perp, \mathbf{r}_\perp\right) \tag{2.12}$$

is the Fourier integral over the one dimensional interval Z_l of layer l;

$$S_l\left(\mathbf{K}_\parallel\right) = \frac{1}{2\pi} \int \mathrm{d}^2\mathbf{r}_\parallel \, \exp\left(-i\mathbf{K}_\parallel \, \mathbf{r}_\parallel\right) \left[\chi_l\left(\mathbf{r}_\parallel\right) - \overline{\chi_l}\right] \tag{2.13}$$

is the two dimensional Fourier transform of $\chi_l\left(\mathbf{r}_\parallel\right)-\overline{\chi}$ where $\mathbf{K}_\parallel$ is the in-plain component of the momentum transfer vector $\mathbf{K}=\mathbf{k}'-\mathbf{k}$. We note that $T_l\left(\mathbf{k}_\perp,\mathbf{k}'_\perp\right)$ can be analytically calculated (See Appendix B)

The off-specularly scattered intensity $I_{\text{off}}=\left(\Psi_{\text{off}},\Psi_{\text{off}}\right)$ is then

$$I_{\text{off}}=\frac{\pi k^4}{2r^2}\sum_{ll'}\left(\Psi^{\text{in}},T_l^\dagger\left(\mathbf{k}_\perp,\mathbf{k}'_\perp\right)S_l^\dagger\left(\mathbf{K}_\parallel\right)S_{l'}\left(\mathbf{K}_\parallel\right)T_{l'}\left(\mathbf{k}_\perp,\mathbf{k}'_\perp\right)\cdot\Psi^{\text{in}}\right), \tag{2.14}$$

which is written as

$$I_{\text{off}}=\frac{\pi k^4}{2r^2}\sum_{ll'}\text{Tr}\left[T_l^\dagger\left(\mathbf{k}_\perp,\mathbf{k}'_\perp\right)S_l^\dagger\left(\mathbf{K}_\parallel\right)S_{l'}\left(\mathbf{K}_\parallel\right)T_{l'}\left(\mathbf{k}_\perp,\mathbf{k}'_\perp\right)\,\rho\right], \tag{2.15}$$

for arbitrary incident polarization, where ρ is the polarization density matrix of the incident radiation.[36] From the convolution theorem, it follows that the Fourier transform $\mathfrak{C}_{ll'}\left(\mathbf{R}_\parallel\right)$ of

$$C_{ll'}\left(\mathbf{K}_\parallel\right)=\frac{1}{2\pi}S_l^\dagger\left(\mathbf{K}_\parallel\right)S_{l'}\left(\mathbf{K}_\parallel\right), \tag{2.16}$$

is the cross-correlation function of the susceptibilities between layers l and l'

$$\mathfrak{C}_{ll'}\left(\mathbf{R}_\parallel\right)=\frac{1}{A}\int\mathrm{d}^2\mathbf{r}_\parallel\,\left[\chi_l\left(\mathbf{R}_\parallel+\mathbf{r}_\parallel\right)-\overline{\chi}_l\right]^\dagger\left[\chi_{l'}\left(\mathbf{r}_\parallel\right)-\overline{\chi}_{l'}\right] \tag{2.17}$$

A being the area of the surface ($A\to\infty$). The final result then becomes

$$I_{\text{off}}=\frac{\pi k^4}{2r^2}\sum_{ll'}\text{Tr}\left[T_l^\dagger\left(\mathbf{k}_\perp,\mathbf{k}'_\perp\right)C_{ll'}\left(\mathbf{K}_\parallel\right)T_{l'}\left(\mathbf{k}_\perp,\mathbf{k}'_\perp\right)\,\rho\right], \tag{2.18}$$

a very convenient expression for randomly distributed lateral inhomogeneities. We note that the off-specular intensity $I_{\text{off}}=I_{\text{off}}\left(\mathbf{K}_\parallel,\mathbf{k}_\perp,\mathbf{k}'_\perp\right)$ is a function of $\mathbf{K}_\parallel$, $\mathbf{k}_\perp$ and $\mathbf{k}'_\perp$, a notation dropped in the calculations. The corresponding values of $\mathbf{K}_\parallel$, $\mathbf{k}_\perp$ and $\mathbf{k}'_\perp$ can be given for the chosen experimental geometry.

A possible experimental realization of the off-specular reflectometry is the so-called 'ω-scan' geometry, where the detector position is set to 2θ and the sample orientation ω on the goniometer is varied. In the special case of ω- scan the in-plain components of the momentum transfer vector $K_\parallel$ and the out-of-plain component of the wave vector of the outgoing wave $k'_\perp$can be expressed by the grazing angle θ and by ω

$$K_\parallel=2k\sin\theta\sin\left(\omega-\theta\right), \tag{2.19}$$

$$k_\perp=k\sin\omega, \tag{2.20}$$

$$k'_{\perp} = -k \sin(2\theta - \omega), \tag{2.21}$$

noting that $K_{\parallel}$ vanish at the specular condition $\omega = \theta$. The full two-dimensional scan in angles ω and 2θ is also used and called '$2\theta - \omega$' -scan. Another widely used arrangement is the so-called 'detector scan' geometry, in which the angle of incidence θ_{in} is fixed, and the scattered intensity is recorded as a function of the outgoing angle, θ_{out}. In case of a detector scan Eqs.(2.19) and (2.24) read

$$K_{\parallel} = k(\cos\theta_{\text{out}} - \cos\theta_{\text{in}}), \tag{2.22}$$

$$k_{\perp} = k \sin\theta_{\text{in}}, \tag{2.23}$$

$$k'_{\perp} = -k \sin\theta_{\text{out}}, \tag{2.24}$$

with the specular condition being $\theta_{\text{out}} = \theta_{\text{in}}$.

III. OFF-SPECULAR SMR

A. Time-differential off-specular SMR

The off-specular intensity in Eq.(2.18) is valid for neutron and x-ray reflectometry, where the time of the scattering process is negligible. However, in case of SMR we detect the time response

$$\Psi_{\text{off}}(\mathbf{r},t) = \frac{1}{\hbar\sqrt{2\pi}} \int_{-\infty}^{\infty} \mathrm{d}E\, \Psi_{\text{off}}(\mathbf{r},E) \exp(-iEt/\hbar), \tag{3.1}$$

after the synchrotron pulse,[37] which is the Fourier transform of the energy-dependent off-specular field. Close to the Mössbauer resonance, both the susceptibilities $\chi_l\left(\mathbf{r}'_{\parallel}, E\right) - \overline{\chi_l}(E)$ and the coherent field $\Psi_{\text{coh}}(\mathbf{r}', E)$ are strongly energy-dependent[37] and, through Eqs.(2.8), (2.12) and (2.13), carry an energy dependence, too, $S_l\left(\mathbf{K}_{\parallel}, E\right)$ and $T_l(\mathbf{k}_{\perp}, \mathbf{k}'_{\perp}, E)$, so that Eq.(2.18) can no longer be applied to calculate the off-specular intensity.

A possible workaround of this problem is to define a distribution function $\Omega_l^{\mu}\left(\mathbf{r}_{\parallel}\right)$ of each homogeneous region $\mu = 1, .., M$ of layer l. This function $\Omega_l^{\mu}\left(\mathbf{r}_{\parallel}\right)$ characterizes the homogeneous regions of layer l of an energy dependent susceptibility $\chi_l^{\mu}(E)$. Over the region of $\chi_l^{\mu}(E)$ the distribution function $\Omega_l^{\mu}\left(\mathbf{r}_{\parallel}\right) = 1$ otherwise $\Omega_l^{\mu}\left(\mathbf{r}_{\parallel}\right) = 0$, so that the

total inhomogeneous susceptibility is the sum

$$\chi\left(\mathbf{r},E\right)=\sum_{\mu=1}^{M}\sum_{l=1}^{S}\Omega_{l}^{\mu}\left(\mathbf{r}_{\parallel}\right)\chi_{l}^{\mu}\left(E\right), \tag{3.2}$$

where the space- and energy-dependent parts of $\chi\left(\mathbf{r},E\right)$ have been separated. The average susceptibility inside layer l reads

$$\overline{\chi_{l}}\left(E\right)=\frac{1}{A}\sum_{\mu=1}^{M}A_{l}^{\mu}\chi_{l}^{\mu}\left(E\right), \tag{3.3}$$

where $A_{l}^{\mu}=\int\mathrm{d}^{2}\mathbf{r}_{\parallel}\,\Omega_{l}^{\mu}\left(\mathbf{r}_{\parallel}\right)$ is the total area of the homogeneous part μ inside layer l. Using (3.2) and (3.3) Eq.(2.13) becomes

$$S_{l}\left(\mathbf{K}_{\parallel},E\right)=\sum_{\mu=1}^{M}G_{l}^{\mu}\left(\mathbf{K}_{\parallel}\right)\chi_{l}^{\mu}\left(E\right), \tag{3.4}$$

with

$$G_{l}^{\mu}\left(\mathbf{K}_{\parallel}\right)=\frac{1}{2\pi}\int\mathrm{d}^{2}\mathbf{r}_{\parallel}\,\exp\left(-i\mathbf{K}_{\parallel}\mathbf{r}_{\parallel}\right)\left[\Omega_{l}^{\mu}\left(\mathbf{r}_{\parallel}\right)-\frac{1}{A}A_{l}^{\mu}\right], \tag{3.5}$$

and finally, the energy-dependent off-specular field in Fraunhofer approximation reads

$$\Psi_{\mathrm{off}}\left(\mathbf{r},E\right)=\sqrt{\frac{\pi}{2}}\frac{k^{2}}{r}\exp\left(ikr\right)\sum_{l,\mu}G_{l}^{\mu}\left(\mathbf{K}_{\parallel}\right)\chi_{l}^{\mu}\left(E\right)T_{l}\left(E\right)\Psi^{\mathrm{in}}, \tag{3.6}$$

while the off-specular intensity is

$$I_{\mathrm{off}}\left(E\right)=\frac{k^{4}}{4r^{2}}\sum_{ll'\mu\mu'}C_{l'l}^{\mu'\mu}\left(\mathbf{K}_{\parallel}\right)\mathrm{Tr}\left[\Gamma_{l'}^{\mu'}\left(E\right)^{\dagger}\Gamma_{l}^{\mu}\left(E\right)\cdot\rho\right]. \tag{3.7}$$

The matrices for the homogeneous region μ, l

$$\Gamma_{l}^{\mu}\left(E\right)=\chi_{l}^{\mu}\left(E\right)T_{l}\left(E\right), \tag{3.8}$$

are the products of the homogeneous solution $T_{l}\left(E\right)$ and the susceptibility $\chi_{l}^{\mu}\left(E\right)$ of that region. For the sake of brevity we have dropped the notation of dependence of T_{l} and Γ_{l}^{μ} on both, $\mathbf{k}_{\perp}$ and $\mathbf{k}'_{\perp}$.

$$C_{l'l}^{\mu'\mu}\left(\mathbf{K}_{\parallel}\right)=\frac{1}{2\pi}G_{l}^{\mu'}\left(\mathbf{K}_{\parallel}\right)^{*}\;G_{l}^{\mu}\left(\mathbf{K}_{\parallel}\right) \tag{3.9}$$

is the geometrical correlation function between layers l and l' , homogeneous parts μ and μ'. In Eq.(3.7) the geometrical correlation function is separated from the energy dependent functions, and can therefore be applied for both time- and energy-domain measurements.

The Fourier transformation can be performed so that with Eq.(3.1) the time dependent intensity becomes

$$I_{\text{off}}(t) = \frac{k^4}{4r^2} \sum_{ll'\mu\mu'} C_{l'l}^{\mu'\mu}\left(\mathbf{K}_{\parallel}\right) \text{Tr}\left[\Gamma_{l'}^{\mu'}(t)^{\dagger}\ \Gamma_{l}^{\mu}(t) \cdot \rho\right], \tag{3.10}$$

where

$$\Gamma_{l}^{\mu}(t) = \frac{1}{\hbar\sqrt{2\pi}} \int_{-\infty}^{\infty} \mathrm{d}E\, \Gamma_{l}^{\mu}(E) \exp\left(-iEt/\hbar\right). \tag{3.11}$$

B. Time-integral off-specular SMR

The time-integrated intensity is $I_{\text{off}}^{\text{int}} = \int_{t_2}^{t_2} \mathrm{d}t\, I_{\text{off}}(t)$, where t_1 and t_2 define the time window of the measurement after the synchrotron bunch. Applying Eqs.(3.10) and (3.11)

$$I_{\text{off}}^{\text{int}} = \frac{k^4}{4\hbar r^2} \sum_{m=-\infty}^{\infty} s_m \int_{-\infty}^{\infty} \mathrm{d}E \sum_{ll'\mu\mu'} C_{l'l}^{\mu'\mu}\left(\mathbf{K}_{\parallel}\right) \text{Tr}\left[\Gamma_{l'}^{\mu'}(E + m\varepsilon)^{\dagger}\ \Gamma_{l}^{\mu}(E)\,\rho\right], \tag{3.12}$$

where $\varepsilon = \frac{h}{t_{\text{bunch}}}$ with t_{bunch} being the time interval between the synchrotron bunches, h is the Planck constant, s_m is the m$^{\text{th}}$ discrete Fourier component of the periodical time window function $S(t) = \sum_{m=-\infty}^{\infty} s_m \exp\left(i\frac{2m\pi}{t_{\text{bunch}}}t\right)$ of the experiment defined by $S(t) = 1$ for $t_1 < t < t_2$, otherwise $S(t) = 0$ after each synchrotron bunch.

IV. APPLICATIONS AND COMPARISON WITH EXPERIMENT

Applying the above theory, off-specular SMR and PNR curves were calculated and compared with the experiment for an MgO/ $[^{57}\text{Fe}\,(2.6\,\text{nm})\,/\text{Cr}\,(1.3\,\text{nm})]_{20}$ antiferromagnetic (AF) multilayer. Due to the strong AF coupling between the iron layers at this spacer thickness one may assume that the domain walls are perpendicular to the surface and run through the multilayer stack from surface to substrate. Model calculation were performed with the following assumptions and parameters. The SMR curves were calculated for the 14.4-keV Mössbauer resonance of ^{57}Fe ($\lambda = 0.086$ nm). The scattering geometry was selected so that the layer magnetizations were parallel/antiparallel to $\mathbf{k}'_{\parallel}$, the condition for the appearance of the SMR specular AF reflection.[13] In case of PNR, a neutron wavelength of $\lambda = 0.1$ nm was assumed. The layer magnetizations were assumed parallel/antiparallel to the neutron spin and perpendicular to $\mathbf{k}'_{\parallel}$. For both, SMR and PNR, the specular intensities were calculated by the free data evaluation computer program EFFI (Environment For FItting).[35,42]

A. Model calculations

The studied MgO/ $[^{57}\mathrm{Fe}\,(2.6\,\mathrm{nm})\,/\mathrm{Cr}\,(1.3\,\mathrm{nm})]_{20}$ ML is a layer antiferromagnet. Consequently, in remanence, the net magnetization of the Fe layers is zero. Moreover, (except for a trivial case of full in-plane saturation) the in-layer magnetization is broken into domains of different orientations resulting in fact in zero layer magnetizations. In the simplest case the situation can be demonstrated by two types of domains, (say type '+' and type '−' domains) separated by 180° domain walls, a situation which can indeed be realized experimentally by an easy axis magnetization of the ML followed by relaxing the field to remanence.[16] In the case of a 1 to 1 surface coverage ratio of the '+' and '− ' type domains averaging the magnetizations within a layer - as mentioned in the introduction - the magnetic contrast is missing, i.e. no AF Bragg peak in the specular reflectometry curves appears. However, when the domain size is comparable to the coherence length (a few times ten to a few thousand nanometers[38]) a net layer magnetization is sampled within the coherence length and a consequent magnetic contrast is seen in the specular reflectometric experiment. Therefore a specific magnetic bias parameter η is introduced by the definition $\eta = A_+/\left(A_+ + A_-\right)$, where A_+ and A_- are the surface areas of the '+' and '−' type domains inside the coherence area within the upper layer. This coherence is smaller then the illuminated area and may have arbitrary position which can be identified by η, therefore we have to average to η. Indeed, the integration in Eq.(2.17) is then performed as a function of η and the off-specular intensity in (2.18) is calculated as

$$I_{\mathrm{off}} = \int_0^1 p\left(\eta\right) I_{\mathrm{off}}\left(\eta\right) \mathrm{d}\eta, \tag{4.1}$$

where $p\left(\eta\right)$ is the normalized probability density of having the magnetic bias parameter η. The upper layer unambiguously identifies the domain structure in the lower layers, since a strict antiferromagnetic out-of-plane correlation is assumed throughout the multilayer stack. For the numerical simulations we assume equal probability of the different configurations and the (4.1) integral is replaced by a discrete sum

$$I_{\mathrm{off}} = \frac{1}{M}\sum_{i=1}^{M} I_{\mathrm{off}}\left(\eta_i\right), \tag{4.2}$$

with $\eta_i = \left(i-1\right)/\left(M-1\right), i = 1..M$ and M being the number of configurations considered in the calculation.

For simplicity, we use an exponential function to describe the correlation of the magnetization directions and interpret the average domain size as the correlation length of this exponential correlation function

$$\mathfrak{C}\left(\mathbf{r}_{\parallel}\right) \sim \exp\left(-\frac{r_{\parallel}}{\xi}\right), \tag{4.3}$$

with ξ being the correlation length.[17] Moreover, the layer and domain type indexes, l and μ, were dropped since the same correlation functions were assumed for each indices, taking into account the alternating sign corresponding to both the strict out-of-plane AF correlation and an in-plane '+'/'−' domain model with 180° domain walls. The Fourier transform of Eq.(4.3) reads

$$C\left(\mathbf{K}_{\parallel}\right) \sim \frac{2\pi\xi^2}{\left[1+\left(K_{\parallel}\,\xi\right)^2\right]^{3/2}}, \tag{4.4}$$

which is then substituted into Eqs.(2.18) and (3.10) for calculating the off-specular PNR and SMR intensities, respectively. Figs. 1 and 2 show the SMR and PNR simulations of the above multilayer, with curves 'a' and 'b' being the specular and off-specular calculations, respectively. The specular curves are typical for AF multilayers, the structural Bragg peaks showing up at $\theta_{\text{in}} = 11.3\,\text{mrad}$ and $\theta_{\text{in}} = 13\,\text{mrad}$ for SMR and PNR, respectively). The AF Bragg peaks appear at $\theta_{\text{in}} = 6.7\,\text{mrad}$ and $\theta_{\text{in}} = 6.5\,\text{mrad}$ for SMR and PNR, respectively). The AF Bragg peaks are small on both specular curves, since the presence of domains decreases the AF contrast between the layers. The Kiessig-type oscillations[39] characteristic of the total thickness of the multilayer are also present on both specular curves, however, due to the strong nuclear resonant absorption, their amplitude is much smaller in case of SMR. Conversely, the absorption of neutrons is negligible, therefore the Kiessig fringes are strong. The simulation in Fig.2 were performed for two different polarizations of the incident neutrons with spin parallel and antiparallel with the direction of magnetization of the majority domains of the top layer. The largest contrast between the curves in Fig.2.a is around the AF Bragg angle, $\theta_{\text{in}} = 6.5\,\text{mrad}$. Below the critical angle, the SMR intensity decreases,[40,41] whereas the PNR curve behaves normally and tends to 1. The off-specular SMR and PNR curves are shown in Figs. 1.b and 2.b, respectively. As seen in Fig.2.b, the off-specular SMR curves are sensitive to the correlation length ξ. Due to geometrical reasons, the frequency of the oscillations on the specular curve in Fig.2.a is twice the frequency of the off-specular case in Fig.2.b. Indeed, following from Eqs.(2.22) and (2.24), any change in θ_{in}

obeying the specular condition $\theta_{\rm out} = \theta_{\rm in}$ causes a change in the perpendicular momentum transfer component that is the double of the change in $\theta_{\rm out}$ with fixed $\theta_{\rm in}$ in the 'detector scan' geometry.

B. Experimental results and discussion

In order to compare Eq.(3.12) with experiments, the two-dimensional '$2\theta - \omega$' SMR scan of a ^{57}Fe/Cr antiferromagnetic multilayer was measured for the first time. Using the 14.4 keV Mössbauer transition of ^{57}Fe nuclei the experiments were performed at the BL09XU nuclear resonance beam line[43] of SPring-8, Japan. The synchrotron was operated in the 203-bunch mode, corresponding to a bunch separation time of $t_{\rm bunch} = 23.6$ ns. The SR was monochromated by a Si(4 2 2)/Si(12 2 2) double channel-cut high resolution monochromator with 6 meV resolution. It was incident on the multilayer specimen downstream mounted in grazing incidence geometry. The delayed radiation was detected using three 2 ns dead time Hamamatsu avalanche photo diodes (APD) in series. These SMR data were time integrated using the time windows given by $t_1 = 1.97$ ns and $t_2 = 21.63$ ns.

The multilayers were prepared under ultra-high vacuum conditions by molecular beam epitaxy at the IMBL facility in IKS Leuven. Preparation and characterization of the MgO(001)/[^{57}Fe/Cr]$_{20}$ multilayer sample has been described earlier.[16,44,45] The layering was verified as epitaxial and periodic, with thicknesses of 2.6 nm for the ^{57}Fe layer, and 1.3 nm for the Cr layer. SQUID magnetometry showed dominantly antiferromagnetic coupling between neighboring Fe layers. According to previous studies on this multilayer,[16,44,45] the magnetizations in Fe align to the (100) and (010) perpendicular easy directions in remanence, respectively corresponding to the (110) and ($\bar{1}$10) directions of the MgO substrate. The layer magnetizations were aligned antiparallel in the consecutive Fe layers by applying a magnetic field (1.6 T) above the saturation value (0.96 T) in the Fe(010) easy direction of magnetization, and then releasing the field to remanence. The alignment is global, the antiferromagnetic domains are only different in the layer sequence of the parallel/antiparallel orientations.[16]

Fig.3 show the two-dimensional '$2\theta - \omega$' SMR scan in the vicinity of the AF-Bragg position. The corresponding simulation for the experimental interval is shown in Fig.4, where the (4.4) correlation function with the correlation length of $\xi = 4.6$ μm was used. Near the specular

line ($2\theta = 2\omega$) the simulation is in good agreement with the experimental data. As stated above, far from the specular direction the (2.6) approximation fails, therefore the simulation less fit to the experimental data.

V. CONCLUSION

Off-specular SMR is sensitive to the lateral structure of the hyperfine fields, therefore it can be used for studying magnetic domains in multilayers. Due to the existing common optical approach, the same theory can be applied for SMR, x-ray reflectometry and polarized neutron reflectometry[26] for both specular and off-specular reflection. Using the perturbative DWBA theory, the off-specularly reflected intensity of SMR is expressed as a function of the geometrical correlation functions of the lateral structure and the specular field profile in the layers. Off-specular SMR and PNR 'detector scan' spectra of an antiferromagnetic $[^{57}\mathrm{Fe}\,(2.6\,\mathrm{nm})\,/\mathrm{Cr}\,(1.3\,\mathrm{nm})]_{20}\,/\mathrm{MgO}$ multilayer were calculated and compared to each other. The two-dimensional '$2\theta - \omega$' SMR scan of the sample was reported and compared with the simulation, the value of the correlation lenth was determined.

APPENDIX A: GENERAL SOLUTION OF THE COHERENT FIELD EQUATION

The solution of Eq.(2.3) was given in Refs.[26,32,35] where, using the derivative field $\Phi_{\mathrm{coh}}(\mathbf{r}_\perp) = (ik\sin\theta)^{-1}\Psi'_{\mathrm{coh}}(\mathbf{r}_\perp)$, the second order differential equation regarding to $\Psi_{\mathrm{coh}}(\mathbf{r})$, was replaced by a set of first order differential equations,[26] providing the solution

$$\begin{pmatrix}\Phi(k_\perp,\mathbf{r}_\perp)\\ \Psi(k_\perp,\mathbf{r}_\perp)\end{pmatrix} = L(k_\perp,\mathbf{r}_\perp)\begin{pmatrix}\Phi(k_\perp,0)\\ \Psi(k_\perp,0)\end{pmatrix}, \tag{A1}$$

where L is the 4×4 characteristic matrix of the system,[26,32,35] $k_\perp = k\sin\theta$ is the out-of-plain component of the wave number vector of the incident plain wave, which latter dependence we drop in this appendix. Here Ψ and Φ are coherent fields, but the 'coh' notation is dropped. The physical meaning of Eq.(A1) is that there is a linear connection expressed by the characteristic matrix L between the fields at depth $\mathbf{r}_\perp = 0$ and at an arbitrary depth $\mathbf{r}_\perp$. Taking into account the boundary conditions, the field at the top surfaces of the system ($\mathbf{r}_\perp = 0$) is

$$\Psi(0) = \Psi^{\mathrm{in}} + R_{\mathrm{sp}}\Psi^{\mathrm{in}}, \tag{A2}$$

the sum of the incident Ψ^{in} and the reflected $R_{\text{sp}}\Psi^{\text{in}}$ waves so Eq.(A1) reads

$$\begin{pmatrix} \Phi(\mathbf{r}_\perp) \\ \Psi(\mathbf{r}_\perp) \end{pmatrix} = L(\mathbf{r}_\perp) \begin{pmatrix} \Psi^{\text{in}} - R_{\text{sp}}\Psi^{\text{in}} \\ \Psi^{\text{in}} + R_{\text{sp}}\Psi^{\text{in}} \end{pmatrix}, \tag{A3}$$

where the concept of impedance tensors was used,[46] taking into account that the fields at $\mathbf{r}_\perp = 0$ are in vacuum (see Eqs.(21) and (22) of Ref.[26]). Expressing the second component from Eq.(A3), the field at an arbitrary depth $\mathbf{r}_\perp$ we have

$$\Psi(\mathbf{r}_\perp) = \left\lfloor L^{[21]}(\mathbf{r}_\perp)(I - R_{\text{sp}}) + L^{[22]}(\mathbf{r}_\perp)(I + R_{\text{sp}}) \right\rfloor \Psi^{\text{in}}, \tag{A4}$$

and using the notation $T(\mathbf{r}_\perp) = L^{[21]}(\mathbf{r}_\perp)(I - R_{\text{sp}}) + L^{[22]}(\mathbf{r}_\perp)(I + R_{\text{sp}})$ the solution of the three dimensional homogeneous wave equation is

$$\Psi_{\text{coh}}(\mathbf{k}, \mathbf{r}) = T(k_\perp, \mathbf{r}_\perp)\, \Psi^{\text{in}} \exp\left(i\mathbf{k}_\parallel \cdot \mathbf{r}_\parallel\right). \tag{A5}$$

APPENDIX B: CALCULATION OF THE $T_l(\mathbf{k}_\perp, \mathbf{k}'_\perp)$ FOURIER INTEGRALS

In this appendix the analytical calculation of the integral (2.12) is given. The 4×4 characteristic matrix[32,46] of an arbitrary homogeneous multilayered film with layers $l = 1, ..., S$ reads

$$L = L_S \cdot ... \cdot L_2 \cdot L_1, \tag{B1}$$

where

$$L_l = \begin{pmatrix} \cosh(kd_l F_l) & \frac{1}{x} F_l \sinh(kd_l F_l) \\ x F_l^{-1} \sinh(kd_l F_l) & \cosh(kd_l F_l) \end{pmatrix}, \tag{B2}$$

is the characteristic matrix of the l^{th} homogeneous layer[26,32] with d_l being the thickness of the l^{th} layer, $x = i \sin\theta$ and the 2×2 matrix $F_l = \sqrt{-I \sin^2\theta - \chi_l}$. We note that L depends on $k_\perp = k \sin\theta$, which dependence is not signed in this Appendix. At depth $\mathbf{r}_\perp$ measured from the top surface of the multilayer the position vector points into layer $j < S$. The interval $\mathbf{r}_\perp$ totally covers the first $j-1$ layers, therefore the characteristic matrix at depth $\mathbf{r}_\perp$ can be written as

$$L(\mathbf{r}_\perp) = L_j(\mathbf{r}_\perp - D_{j-1}) \cdot L_{(j-1)}, \tag{B3}$$

where $D_{j-1} = \sum_{l=1}^{j-1} d_l$ is the total thickness of layers up to layer $j-1$ and $L_{(j-1)} = L_{j-1} \cdot ... \cdot L_1$ is the characteristic matrix of layers $1, .., j-1$. We note that layer j is only partially covered

by the depth interval, which is indicated by the argument $(\mathbf{r}_\perp - D_{j-1})$ in Eq.(B3) instead of the total thickness d_j. It is also important to note that $L(\mathbf{r}_\perp)$ depends on the thicknesses and susceptibilities of all the covered layers and furthermore it also depends on the angle of grazing incidence θ.

Using Eqs.(2.8), (B2) and (B3) the integral (2.12) can be analytically calculated. Indeed, the two integrals

$$I_j^+ = \frac{1}{\sqrt{2\pi}} \int\limits_{Z_j} \mathrm{d}\mathbf{r}_\perp \exp\left(-i\mathbf{k}'_\perp \mathbf{r}_\perp\right) \sinh\left[k\left(\mathbf{r}_\perp - D_{j-1}\right) F_j\right] \tag{B4a}$$

$$I_j^- = \frac{1}{\sqrt{2\pi}} \int\limits_{Z_j} \mathrm{d}\mathbf{r}_\perp \exp\left(-i\mathbf{k}'_\perp \mathbf{r}_\perp\right) \cosh\left[k\left(\mathbf{r}_\perp - D_{j-1}\right) F_j\right] \tag{B4b}$$

results

$$I_j^+ = \alpha_j + \beta_j \tag{B5a}$$

$$I_j^- = \alpha_j - \beta_j, \tag{B5b}$$

with

$$\alpha_j = \exp\left(-i\mathbf{k}'_\perp D_{j-1}\right) \cdot \left\{\left(kF_j - i\mathbf{k}'_\perp I\right)^{-1} \exp\left[\frac{d_j}{2}\left(kF_j - i\mathbf{k}'_\perp I\right)\right] \sinh\left[\frac{d_j}{2}\left(kF_j - i\mathbf{k}'_\perp I\right)\right]\right\} \tag{B6a}$$

$$\beta_j = \exp\left(-i\mathbf{k}'_\perp D_{j-1}\right) \cdot \left\{\left(kF_j + i\mathbf{k}'_\perp I\right)^{-1} \exp\left[-\frac{d_j}{2}\left(kF_j + i\mathbf{k}'_\perp I\right)\right] \sinh\left[\frac{d_j}{2}\left(kF_j + i\mathbf{k}'_\perp I\right)\right]\right\}. \tag{B6b}$$

Finally the required expression reads

$$T_l\left(\mathbf{k}_\perp, \mathbf{k}'_\perp\right) = \left[xF_j^{-1} I_j^+ L_{(j-1)}^{[11]} + I_j^- L_{(j-1)}^{[21]}\right](I - R_{\mathrm{sp}}) + \left[xF_j^{-1} I_j^+ L_{(j-1)}^{[12]} + I_j^- L_{(j-1)}^{[22]}\right](I + R_{\mathrm{sp}}). \tag{B7}$$

Eq.(B8) is physically the Fourier transform of the depth profile function of the coherent field and we note again the dependence on $\mathbf{k}_\perp$.

ACKNOWLEDGMENTS

This work was partly supported by the Hungarian Scientific Research Fund (OTKA) under Contract Nos. T029409 and T047094 as well as by the European Community under the

Specific Targeted Research Project Contract No. NMP4-CT-2003-001516 (DYNASYNC). The authors gratefully acknowledge the beam time supplied free of charge by the Japan Synchrotron Radiation Institute (JASRI) for experiment No: 2002B239-ND3-np. Our gratitude goes to *Dr. A.Q. Baron* (SPring-8, JASRI) for kindly supplying the fast Hammamatsu APD detectors, *Dr. Johan Dekoster* (IKS Leuven) for preparing the multilayer samples for the experiment and to *Mr. Daniel Merkel* for the assistance in the data processing. One of the authors (LD) gratefully acknowledges the financial support by the Deutscher Akademischer Austauschdienst (DAAD).

---

* Electronic address: deak@rmki.kfki.hu

[1] M. Lax, Rev. Mod. Phys. 23 (1951) 287.

[2] X.-L. Zhou, S.-H. Chen, Phys. Rep. 257 (1995) 223.

[3] G.P. Felcher, Physica B 192 (1993) 137.

[4] C.F. Majkrzak, Physica B 173 (1991) 75.

[5] S.K. Sinha, Physica B 173 (1991) 25.

[6] J.P. Hannon, G.T. Trammell, M. Blume, and Doon Gibs, Phys. Rev. Lett. 61 (1988) 1245.

[7] D.B. Mac Whan, J. Synchrotron Radiat. 1 (1994) 83., and references therein.

[8] T.P.A. Hase, I. Pape, B.K. Tanner, H. Dürr, E. Dudzik, G. van der Laan, C.H. Marrows and B.J. Hickey, Phys. Rev. B 61 (2000) R3792.

[9] V. Lauter-Pasyuk, H.J. Lauter, B. Toperverg, O. Nikonov, E. Kravtsov, M.A. Milyaev, L. Romashev and V. Ustinov, Physica B 283 (2000)194.

[10] S. Langridge, J. Schmalian, C.H. Marrows, D.T. Dekadjevi and B.J. Hickey, Phys. Rev. Lett. 85 (2000) 4964.

[11] D.L. Nagy, L. Bottyán, L. Deák, E. Szilágyi, H. Spiering, J. Dekoster and G. Langouche, Hyp. Int. 126 (2000) 353.

[12] T.L. Toellner, W. Sturhahn, R. Röhlsberger, E.E. Alp, C.H. Sowers and E.E. Fullerton, Phys. Rev. Lett. 74 (1995) 3475.

[13] A.I. Chumakov, L. Niesen, D.L. Nagy and E.E. Alp, Hyp. Int. 123/124 (1999) 427.

[14] L. Deák, L. Bottyán, M. Major, D.L. Nagy, H. Spiering, E. Szilágyi and F. Tanczikó, Hyp. Int. 144/145 (2002) 45.

[15] R. Röhlsberger, J. Bansman, V. Senz, K.L. Jonas, A. Bettac, K.H. Meiwes-Broer, Phys. Rev. B. 67 (2003) 245412.

[16] D.L. Nagy, L. Bottyán, B. Croonenborghs, L. Deák, B. Degroote, J. Dekoster, H.J. Lauter, V. Lauter-Pasyuk, O. Leupold, M. Major, J. Meersschaut, O. Nikonov, A. Petrenko, R. Rüffer, H. Spiering and E. Szilágyi, Phys. Rev. Lett. 88 (2002) 157202.

[17] S.L. Sinha, E.B. Sirota, S. Garoff, H.B. Stanley, Phys. Rev B 38 (1988) 2297.

[18] B.T. Toperverg, Physica B 297 (2001) 160;

[19] B.T. Toperverg, O. Nikonov, V. Lauter-Pasyuk, H.J. Lauter, Physica B 297 (2001) 169.

[20] V. Lauter-Pasyuk at al., J. Magn. Magn. Mater. 226-230 (2001) 1694.

[21] A. Rühm, B.T. Toperverg, H. Dosch, Phys. Rev. B. 60 (1999) 16073.

[22] George H. Vineyard, Phys. Rev. B. 26 (1982) 4146.

[23] G.P. Felcher, R.O. Hilleke, R.K. Crawford, J. Haumann, R. Kleb, and G. Ostrowski, Rev. Sci. Instrumm 58 (1987) 609.

[24] L.G. Parratt, Phys. Rev. 95 (1954) 359.

[25] C.F. Majkrzak, Physica B 156\&157 (1989)619.

[26] L. Deák, L. Bottyán, D.L. Nagy, and H. Spiering, Physica B 297 (2001) 113.

[27] A.M. Afanas'ev and Yu. Kagan, Sov. Phys. —JETP 21 (1965) 215.

[28] J.P. Hannon and G.T. Trammell, Phys. Rev. 186 (1969) 306.

[29] J.P. Hannon, G.T. Trammell, M. Mueller, E. Gerdau, R. R üffer, and H. Winkler, Phys. Rev. B 32 (1985) 6363.

[30] S.M. Irkaev, M.A. Andreeva, V.G. Semenov, G.N. Belozerskii and O.V. Grishin, Nucl. Instrum. Methods B 74 (1993) 545.

[31] S.M. Irkaev, M.A. Andreeva, V.G. Semenov, G.N. Beloserskii, and O.V. Grishin, Nucl. Instrum. Methods B 74 (1993) 554.

[32] L. Deák, L. Bottyán, D.L. Nagy and H. Spiering, Phys. Rev. B. 53 (1996) 6158.

[33] R. Röhlsberger, Hyp. Int. 123/124 (1999) 301.

[34] R. Röhlsberger, Hyp. Int. 123/124 (1999) 455.

[35] H. Spiering, L. Deák, and L. Bottyán, Hyp. Int. 125 (2000) 197.

[36] M. Blume and O.C. Kistner, Phys. Rev. 171 (1968) 417.

[37] G.T Trammell and J.P. Hannon, Phys. Rev B 18 (1979) 165.

[38] A. Q. R. Baron, A. I. Chumakov, H. F. Grünsteudel, H. Grünsteudel, L. Niesen, and R. Rüffer,

PRL 77 (1996) 4808.

[39] H. Kiessig, Annalen der Physik (1931) 769.

[40] L. Deák, L. Bottyán, D.L. Nagy, Hyp. Int. 92 (1994)1083.

[41] A.Q.R. Baron, J. Arthur, S.L. Ruby, A.I. Chumakov, G.V. Smirnov, G.S. Brown, Phys. Rev. B **50,** (1994) 10354.

[42] The computer program EFFI is available from ftp://nucssp.rmki.kfki.hu/pub/effi

[43] Y. Yoda, M. Yabashi, K. Izumi, X.W. Zhang, S. Kishimoto, S. Kitao, M. Seto, T. Mitsui, T. Harami, Y. Imai, and S. Kikuta, Nucl. Instrum. Methods Phys. Res. A **467**, (2001) 715.

[44] L. Bottyán, L. Deák, J. Dekoster, E. Kunnen, G. Langouche, J. Meersschaut, M. Major, D.L. Nagy, H.D. Rüter, E. Szil ágyi, K. Temst, J. Magn. Magn. Mater. **240**, (2002) 514.

[45] F. Tancziko, L. Deák, D.L. Nagy, L. Bottyán, Nucl. Instr. Meth. Phys. Res. B **226**, (2004) 461.

[46] G.M. Borzdov, L.M. Barskovskii, and V.I. Lavrukovich, Zh. Prikl. Spektrosk. 25 (1976) 526.

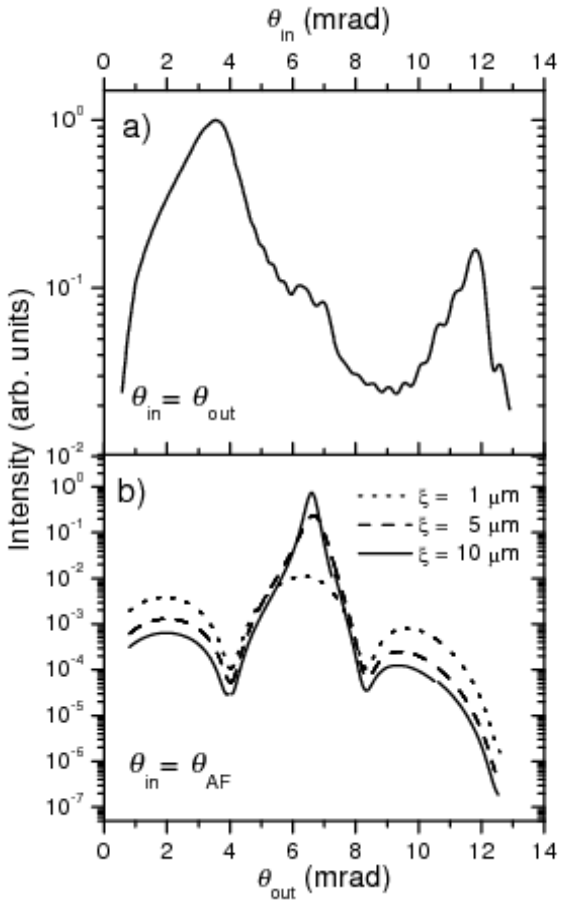

FIG. 1: Specular (a) and off-specular Synchrotron Mössbauer reflectometry curves of $\left[^{57}\mathrm{Fe}\,(2.6\,\mathrm{nm})\,/\mathrm{Cr}\,(1.3\,\mathrm{nm})\right]_{20}/\mathrm{MgO}$ antiferromagnetic multilayer(calculated for the 14.4-keV Mössbauer resonance of ^{57}Fe, with wavelength $\lambda = 0.086$ nm). The off-specular intensity is calculated for three different correlation lengths ξ with the incident angle θ_{in} fixed at the antiferromagnetic Bragg position. We have set a 33% majority of the '+' type domains in the model.

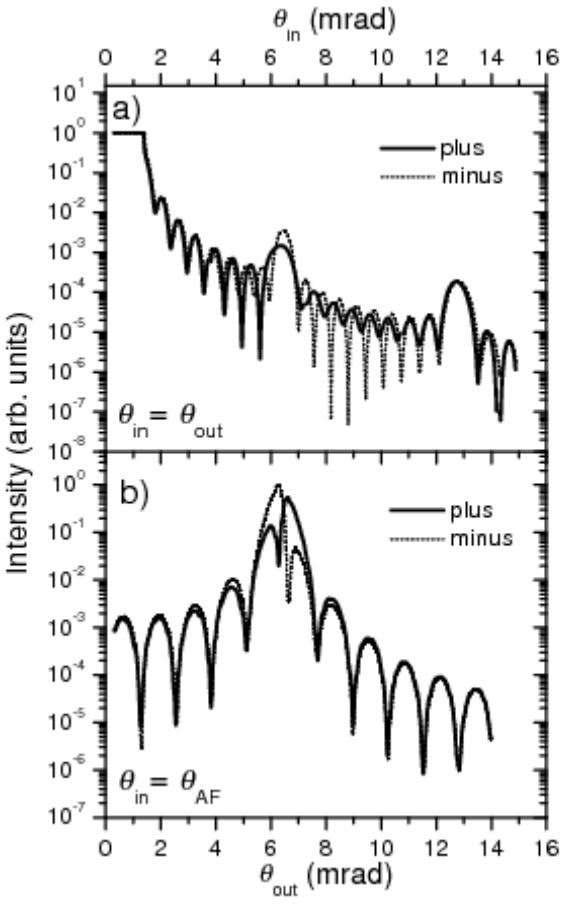

FIG. 2: Specular (a) and off-specular Polarized Neutron Reflectometry curves of $\left[^{57}\mathrm{Fe}\,(2.6\,\mathrm{nm})\,/\mathrm{Cr}\,(1.3\,\mathrm{nm})\right]_{20}/\mathrm{MgO}$ antiferromagnetic multilayer (with neutron wavelength of $\lambda = 0.1$ nm). The off-specular intensity is calculated for the incident angle θ_{in} fixed to the AF Bragg position. The solid and dashed lines show the calculations for two different incident polarizations of neutrons, where notations 'plus' and 'minus' indicate the neutron polarizations parallel and antiparallel to the the magnetization of the '+' type domains of the 1^{st} layer, respectively. We have set a 33% majority of the '+' type domains and used $\xi = 10$ μm correlation length in the model.

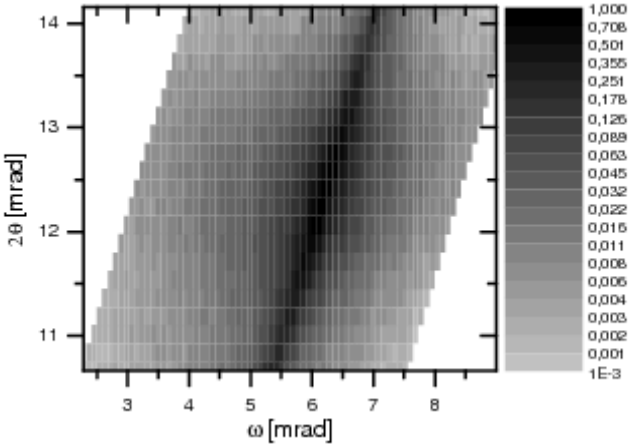

FIG. 3: Two-dimensional off-specular Synchrotron Mössbauer reflectometry map of $\left[^{57}\mathrm{Fe}\,(2.6\,\mathrm{nm})\,/\mathrm{Cr}\,(1.3\,\mathrm{nm})\right]_{20}$ /MgO antiferromagnetic multilayer around the first AF-Bragg peak measured in the ' $2\theta-\omega$ scan' geometry. The intensities are shown on the logarithmic color scale and are normalized.

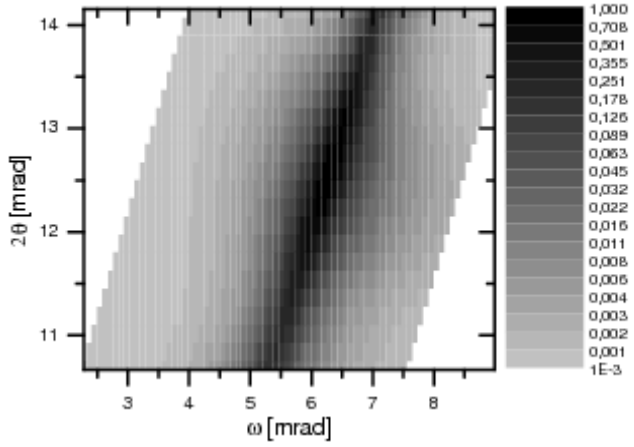

FIG. 4: Symulated off-specular Synchrotron Mössbauer reflectometry map of $\left[^{57}\mathrm{Fe}\,(2.6\,\mathrm{nm})\,/\mathrm{Cr}\,(1.3\,\mathrm{nm})\right]_{20}$ /MgO antiferromagnetic multilayer around the first AF-Bragg peak using the '$2\theta-\omega$ scan' geometry. $\xi = 4.6$ μm correlation length was used in the model. The intensities are shown on the logarithmic color scale and are normalized.